NASA Technical Memorandum 100129

Imaging Subtle Microstructural Variations in Ceramics With Precision Ultrasonic Velocity and Attenuation Measurements

Edward R. Generazio, Don J. Roth, and George Y. Baaklini
Lewis Research Center
Cleveland, Ohio

November 1987

National Aeronautics and
Space Administration

Lewis Research Center
Cleveland, Ohio 44135

Summary

Acoustic images of silicon carbide ceramic disk were obtained using a precision scanning contact pulse echo technique. Phase and cross-correlation velocity, and attenuation maps were used to form color images of microstructural variations. These acoustic images reveal microstructural variations not observable with x-ray radiography.

Introduction

There is an international research effort to incorporate ceramic components into hot sections of heat engines. A major portion of this effort is directed towards the understanding and control of ceramic processing so that the strength of ceramics may be optimized. To date, the strength of sintered ceramics (e.g., SiC) is well below, by about two orders of magnitude, the theoretical strength (refs. 1 and 4). This discrepancy is understood to be due to the presence of voids, inclusions, agglomerates, and anomalously large grains (ref. 4). These defects, causing premature failure, are introduced or formed during the ceramic manufacturing process. Considerable work has already been done to remove these strength reducing material variations. This has resulted in a steady increase in the fracture strength of ceramics, however, the rate of this increase has slowed. Adding to the problem is the fact that the fracture strength of identically produced experimental samples varies as much as 35 percent (ref. 2). As a result of the loss of momentum toward higher strengths, researchers are turning to ceramic-ceramic fiber composites. These composites show promise of increasing the fracture strength of ceramic materials even further. It is likely that the same material strength variations will be present, at least locally in the matrix, in ceramic composites. Therefore, before abandoning monolithic ceramics for ceramic composites, it would seem appropriate to investigate the origin of these strength reducing defects causing the disparity between the experimental and theoretical fracture strengths for monolithic ceramics. The wide spread in the fracture strengths of identically produced samples is quite troublesome and is of particular interest.

The work shown here is aimed at precision measurement of material variations. The variations that we will be most concerned with are subtle porosity and grain size distribution variations that occur during processing. These variations are essentially unobservable using standard evaluation techniques such as optical or x-ray analysis. These subtle variations may collectively lead to the creation of critical sized pores, grains, or agglomerates.

In order to measure material variations with precision we need a probe that will interact with these variations. Optical and x-ray analysis are believed to yield sufficiently accurate results. This is well supported with past and current research results in metals. It should be pointed out that metals also have fracture strengths well below their theoretical strengths. This has been attributed to the presence of dislocations in the metals. Ceramics are extremely sensitive to even slight variations in the microstructure. Direct observation and determination of localized failure sites (usually identified to be isolated pores, inclusions, agglomerates, and anomalously large grains) have shown the importance of these material variations (ref. 4). These failure sites cannot be determined a priori by optical and x-ray methods. It seems plausible that these failure causing variations do not occur spontaneously in isolation but are the result of processing variations or history of processing variations of the environment that surrounds them.

Ultrasonic waves interact substantially with pores, grains, agglomerates, and inclusions. For this reason, ultrasound is chosen as a probe for microstructural variations. Ultrasonic imaging has been used successfully for many years. Imaging techniques such as C-scans for materials and medical sonoscans have proved to be useful. These imaging techniques are imprecise and not sufficiently sensitive to reveal subtle changes in microstructure.

In this work we will demonstrate that by using precise and accurate ultrasonic measurements, microstructural variations unobservable by x-ray techniques can be revealed. These microstructural variations are likely to be present in all sintered ceramic materials.

Interaction of Ultrasonic Waves with Material Variations

Ultrasonic waves are known to interact with both pores and grains existing in materials. Physically each pore or grain acts as an acoustic scattering site that removes energy from the impeding ultrasonic wave. Additionally, the velocity of the ultrasonic wave is found to be linearly dependent on the bulk density (refs. 5 and 6), while independent of the grain size in a polycrystalline solid.

The use of pulse-echo techniques is well established. The configuration is shown in figure 1(a). A single broadband ultrasonic pulse (main pulse) is excited (via the crystal) in the buffer rod. The ultrasonic pulse is partially reflected at the buffer rod-couplant-sample (BCS) interface. The first front-surface reflected pulse is labeled FS_2 in figure 1(a). The main pulse travels forward through the sample and then reflects off the back surface of the sample and again interacts with the BCS interface. This first back-surface reflection is labeled B_1'. Echo B_1' is partially reflected at the BCS interface and is subsequently reflected again at the back surface. The second back-surface reflection is labeled B_2'. Echo's B_1' and B_2' are not directly measurable with the BCS configuration. Their reduced waveform amplitudes, labeled B_1 and B_2 in figure 1(b), are measurable.

Attenuation

The attenuation coefficient for this experimental configuration is given by

$$\alpha(f) = \frac{1}{2\,\Delta X} \ln \left\{ \frac{|B_1(f)|\,|R(f)|}{|B_2(f)|} \right\}$$

with

$$|R(f)| = \left| \frac{FS_2(f)}{FS_1(f)} \right|$$

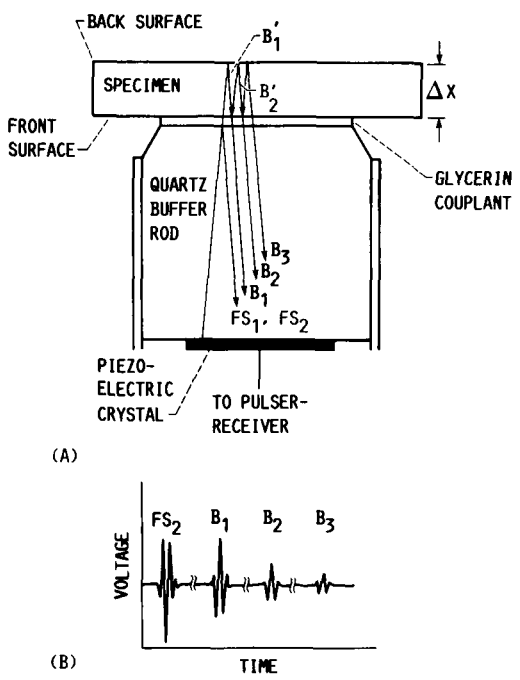

Figure 1.—Diagram of transducer/specimen configuration for pulse echo ultrasonics. (CD-87-26970)

$|FS_1(f)|$ and $|FS_2(f)|$ are the Fourier spectra of the first front-surface reflection without and with the sample present on the buffer rod, respectively. $|R(f)|$ is the frequency dependent BCS reflection coefficient (ref. 7). $|B_1(f)|$ and $|B_2(f)|$ are the Fourier spectra of pulses B_1 and B_2, respectively. ΔX is the thickness of the sample.

Ultrasonic Velocity

There are several ways to measure the velocity with the BCS configuration. Peak detection, echo overlap, cross correlation, and phase methods are available (refs. 8 and 9). Both peak detection and echo overlap are the most common used, however, they are rather imprecise. These two techniques are accurate if the ultrasonic pulse shape is not distorted as it traverses the sample. They should not be expected to yield accurate results for most acoustically dispersive materials where the pulse shape is often distorted as it travels through the material. Cross correlation is probably somewhat better than the previous two in that it may be used with noisy signals such as those found with composites. It is, nevertheless "essentially" a mathematical formulation of echo overlap. Phase velocity is the velocity at a particular frequency and is most often expressed as velocity as a function of frequency. The determination phase velocity is independent of the pulse shape and will yield accurate results for both nondispersive and dispersive materials.

Since phase and cross-correlation velocities are probably the most accurate of the four we will use these for the formation of images constructed by mapping velocity over the specimen.

The cross-correlation velocity is given by

$$V = \frac{2\,\Delta X}{\tau_0}$$

where τ_0 is the time shift for which

$$\left| \lim_{T \to \infty} \int_{-T}^{T} B_1(t) \bullet B_2(t + \tau)dt \right| \quad -\infty \le \tau \le \infty$$

reaches a maximum value.

The phase velocity is given by

$$V(f) = \frac{(2\,\Delta X)2\pi f}{|\Delta\theta|}, \qquad \Delta\theta = \theta_2 - \theta_1$$

with

$$\theta_1(f) = \tan^{-1} \left\{ \frac{\mathcal{Im}\,(B_1(f))}{\mathcal{Re}\,(B_1(f))} \right\}$$

and

$$\theta_2(f) = \tan^{-1}\left\{\frac{\mathcal{Im}\,(B_2(f))}{\mathcal{Re}\,(B_2(f))}\right\}$$

Experimental

Samples

Two disks 38 mm diameter by 4 mm were produced using standard ceramic processing techniques. The samples were sintered 0.5 hr at 2090 and 2190 °C yielding densities of 2.97 and 3.12 gm/cm^3, respectively. (The theoretical density for these samples is 3.2 gm/cm^3.) After sintering the disks were machined to ± 0.0011 cm. One side of each disk was polished to a mirror finish with 3 μm diameter diamond slurry. The polishing was done to reduce the acoustic reflection coefficient that subsequently increased the accuracy of the ultrasonic measurement (ref. 7).

Radiography

Radiographs of the samples investigated were made using both conventional and microfocus techniques. Two methods were used in an effort to obtain the best, highest contrast, radiographs. The results of the two methods were similar. The microfocus radiograph is magnified (as obtained) for contact print processing and for this reason was chosen for comparison with ultrasonic data. The radiographs were made with a molybdenum target with 17 to 21 keV photon energies.

Acoustic Scanning Setup

The disks were mounted in a polymethalmethacrylate sample holder as shown in figure 2. A large O-ring was glued to the underside of the sample holder. The sample holder was mounted on a computer controlled X-Y-Z position microscanning table having a step resolution of 1.0 μm in the X, Y, and Z directions. All scans were done in a 46 by 46 point array with each point separated by 1000 μm. Above the microscanning table, a 100 MHz broadband transducer having a 1/4 in. diameter buffer rod and 1/8 in. diameter piezoelectric crystal was mounted on a displacement pressure gauge. The contact pressure was 10 ± 0.1 lb.

Data Acquisition, Instrument Control, and Analysis

It is common to have a computer control movement of instruments, acquire data, and analyze the data. This often excessively burdens the computer and subsequently the researcher forfeits resolution and/or accuracy of the data in order to reduce the acquisition and analysis time and the data storage space required. A problem that pushes the researcher in this direction, is that computer control of instruments and data acquisition is easily done in Basic programming language with standard general purpose interface buss (GPIB) instrument

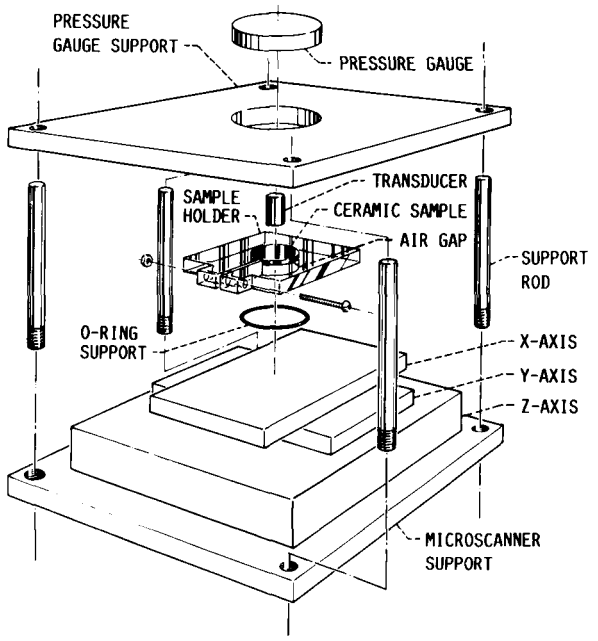

Figure 2.—Diagram of experimental setup used for scanning ceramic samples. (CD-87-26663)

interface software. This results in a Basic data file that is ready to be analyzed using Basic language mathematics. Fortran programming language would be a more efficient language for this analysis. Computers that are dedicated to instrument control and data acquisition are usually single user systems with one operating system and one programming language. So that, conversion of Basic data files to Fortran data files for high-speed analysis is of little use unless an alternate computer system with Fortran is available.

To optimize the data acquisition and analysis two computers were interfaced for this work. A block diagram of the interface arrangement is shown in figure 3. Computer B is programmed using Basic language to perform all the instrument control and data acquisition. Computer A contains an array processor (for fast Fourier transforms) and is programmed using Fortran language to perform all the analysis. The acquired data (512

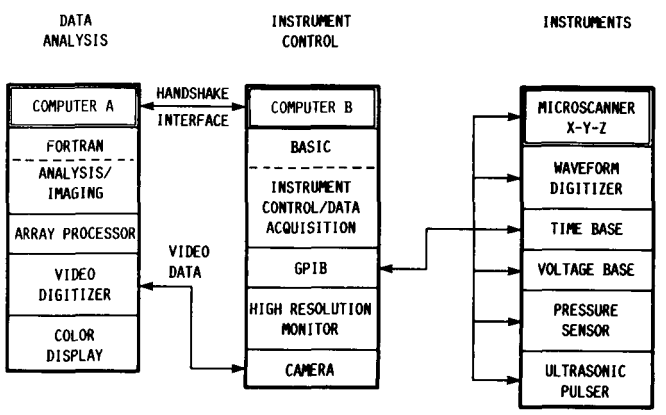

Figure 3.—Diagram of computer configuration used for signal acquisition and analysis. (CD-87-26971)

ORIGINAL PAGE
COLOR PHOTOGRAPH

point waveform) in computer B is then sent to computer A. A handshake interface between the two computers controls the flow and checks the integrity of the data. The conversion of Basic data to Fortran data is done by an analog video interface.

Results

The first set of data (figs. 4 to 10) are for the sample sintered at 2090 °C. The radiograph (fig. 4) indicates that the sample is relatively uniform in density. Slight variations can be identified by the trained eye just to the lower left of the center of the sample.

The cross-correlation velocity image (fig. 5) reveals different results from the radiograph. There exists a low-speed area (cloud) near the center of the sample. A velocity scan horizontally across the center of the sample is shown in the figure. The velocity increases fairly uniformly from the center of this cloud out of the edge of the sample. The highest velocities are at the outer edge. The cross-correlation velocity varies from 1.12 to 1.15 cm/μs or about 2.6 percent over the entire sample.

The phase velocity at 100 MHz (fig. 6) reveals a more detailed picture of the velocity changes over the sample. This image indicates that the velocity is varying nonuniformly over the sample. A velocity scan horizontally across the center of the sample is shown in the figure. The velocity oscillates between higher and lower speeds in the center of the sample with the highest velocities at the outer edge. The phase velocity varies from 1.07 to 1.15 cm/μs or about 8 percent over the entire sample.

The attenuation at 80 MHz is shown in figure 7. The crescent area on the right hand side represents a region having higher attenuation than the central region. The extreme left reveals a curved shaped attenuation band where the attenuation is similar to the central region. The attenuation at 80 MHz varies from 0.0 to 2.0 Np/cm over the sample. Zero attenuation corresponds to an unmeasurable low attenuation for this frequency and experimental configuration.

At 100 MHz (fig. 8) the relatively uniform crescent region on the right hand side of the image obtained at 80 MHz (fig. 7)

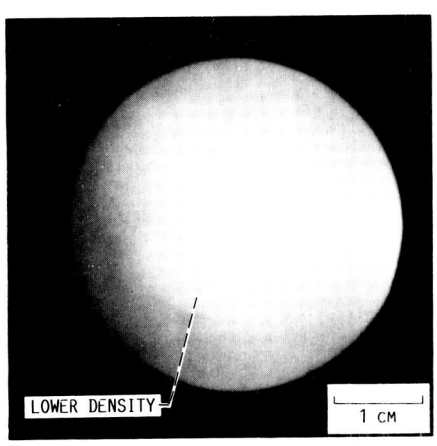

Figure 4.—Microfocus x-ray radiograph of SiC disk sintered at 2090 °C. (CD-87-26973)

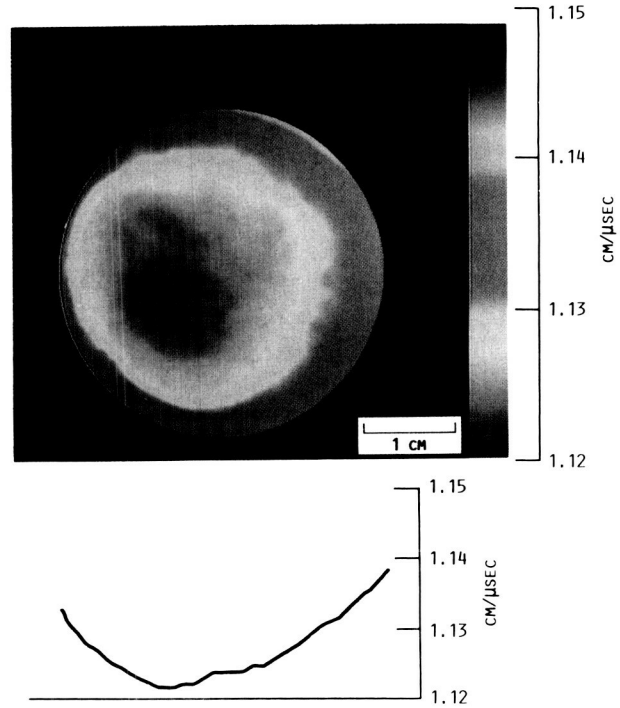

Figure 5.—Cross correlation velocity map of SiC disk sintered at 2090 °C. (CD-87-26969)

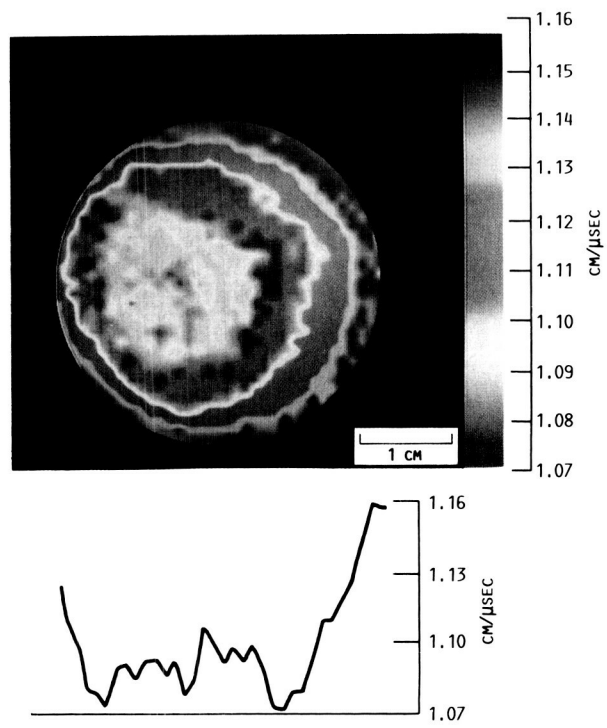

Figure 6.—Phase velocity map of SiC disk sintered at 2090 °C. (CD-87-26960)

ORIGINAL PAGE
COLOR PHOTOGRAPH

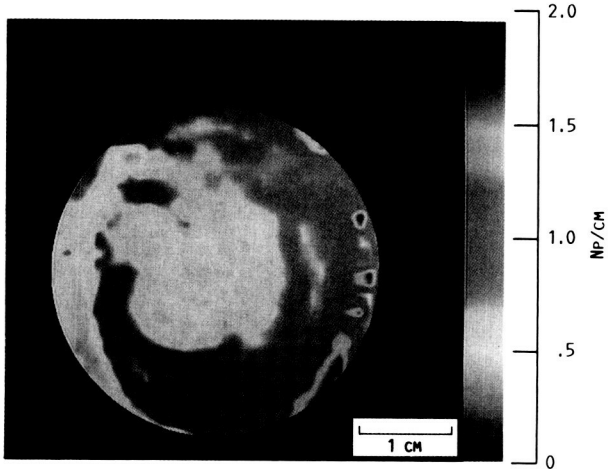

Figure 7.—Attenuation map at 80 MHz for SiC disk sintered at 2090 °C. (CD-87-26966)

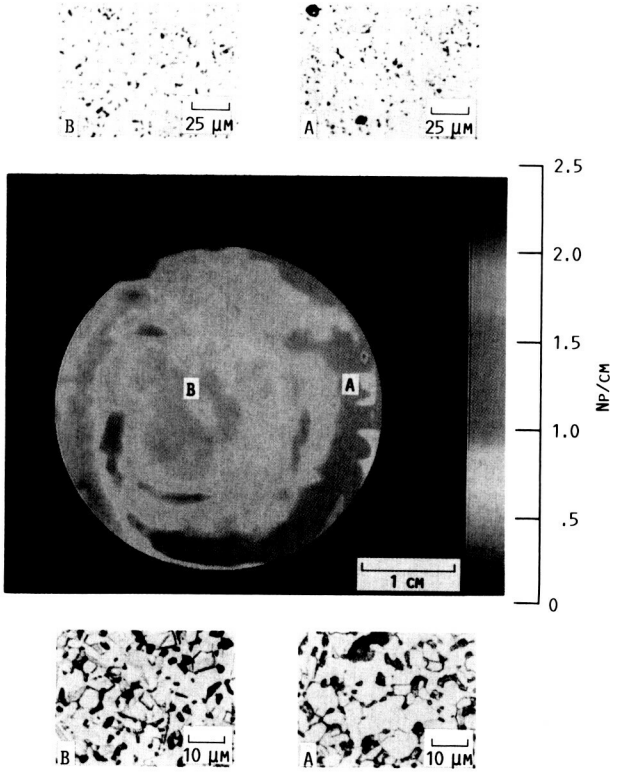

Figure 8.—Attenuation map at 100 MHz and microstructure for SiC disk sintered at 2090 °C. (CD-87—26964)

now exhibits oscillations in the attenuation that give a spiral galaxy appearance. Note also that the scale is different from the image obtained at 80 MHz. The microstructure at point A and B is also shown in figure 8. The ultrasonic direction is vertical. An estimate of the porosity fraction can be made, from the photomicrographs (upper two) of the unetched areas, by determining the ratio of dark areas (pores) to the total area containing these pores. For points A and B these ratios are 0.12 and 0.17, respectively. This indicates that the central region is more porous than the outer right hand side edge. The pore size at point B is about 1 to 5 μm. Pores about five times larger (15 μm) appear scattered throughout the region at point A. The grain size (lower two photomicrographs) at both points A and B is approximately the same at 5 to 10 μm.

The attenuation at 120 MHz (fig. 9) shows a larger central region. The highest attenuation appears as a crescent area on the right hand side edge. The lowest attenuation areas are identified as a crescent area on the left hand side and a central region having a radius of one-half the sample diameter.

As indicated previously, the reflection coefficient can be optimized to obtain the most accurate results. The reflection coefficient is shown in figure 10. The reflection coefficient over the entire sample ranges from 0.37 to 0.63. This reflection coefficient, obtained by mirror polishing the sample, yields the most accurate data. Reflection coefficients above 0.8 or below 0.2 result in increased uncertainties in the observed attenuation (ref. 7).

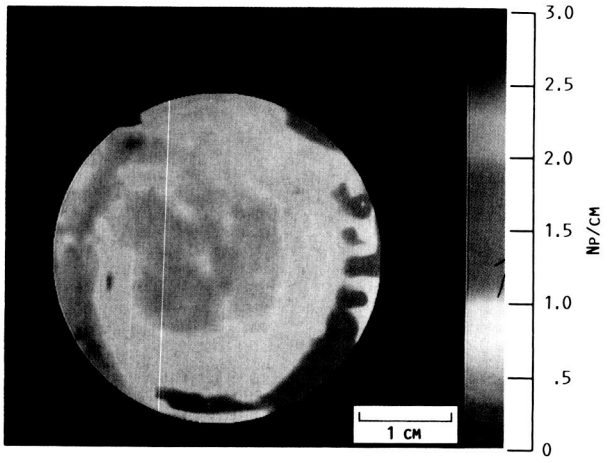

Figure 9.—Attenuation map at 120 MHz for SiC disk sintered at 2090 °C. (CD-87—26968)

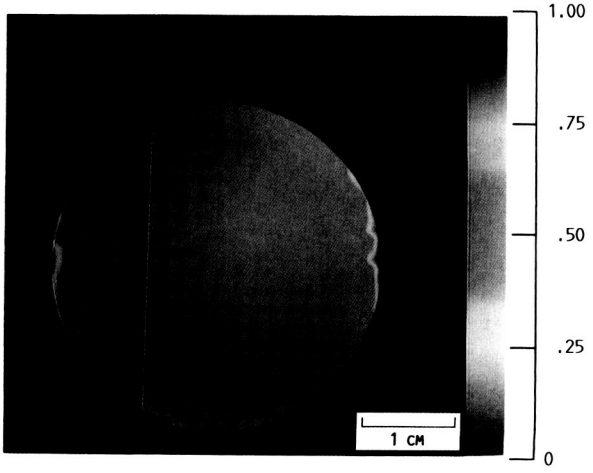

Figure 10.—Reflection coefficient map at 100 MHz for SiC disk sintered at 2090 °C. (CD-87-26967)

ORIGINAL PAGE
COLOR PHOTOGRAPH

The next set of data (figs. 11 to 16) are for the sample sintered at 2190 °C. The radiograph (fig. 11) reveals a low-density region at the center and extends to the top, left, and lower left. There is a high-density crescent-shaped area, on the right side, that extends to form a ring around the outer edge of the sample. Some higher density strands are present in the central low-density region.

The cross-correlation velocity (fig. 12) reveals a low-speed region in the same position as the low-density region of the x-ray data. Two features can be observed, within this low-speed area, at the same location as the high-density strands in the x-ray data. The velocity horizontally across the center of the sample is also shown in the figure. The velocity is relatively uniform in the low-speed region and increases rapidly near the edge of this low-speed area. The cross correlation varies from 1.13 to 1.27 cm/μs or about 12 percent.

Figure 11.—Microfocus x-ray radiograph of SiC disk sintered at 2190 °C. (CD-87-26972)

The 100 MHz phase velocity (fig. 13) again reveals a more detailed picture. The phase velocity horizontally across the center of the sample reveals a complicated oscillatory structure with a low-speed center surrounded by a higher speed donut-shaped ring. The outer edge of the low-speed region is surrounded by isolated and connected very high-speed areas. The phase velocity varies from 1.12 to 1.24 cm/μs or about 10 percent.

The attenuation at 100 MHz (fig. 14) shows a high attenuation region at the same position as the low-density region of the x-ray data. This high attenuation area has a complicated structure where the attenuation varies rapidly with position from 0.0 to 4.0 Np/cm. The attenuation in the crescent-shaped area on the right hand side is unmeasurably low.

The microstructure at points A and B is shown in figure 14. The porosity fraction for points A and B is 0.02 and 0.17, respectively. As in the previous sample the central region is more porous. Note that for point B (top photomicrograph) the left hand side of the photomicrograph exhibits a lower porosity than the right hand side of the photomicrograph. The pore sizes are in the range 2 to 10 μm. This extreme local variation in porosity was observed horizontally across the high attenuating region. At point A the microstructure is nearly fully dense with sparse large pores being about 3 μm. The grain size at points A and B were similar at about 5 to 15 μm. Several anomalously large grains (fig. 15) were found scattered across

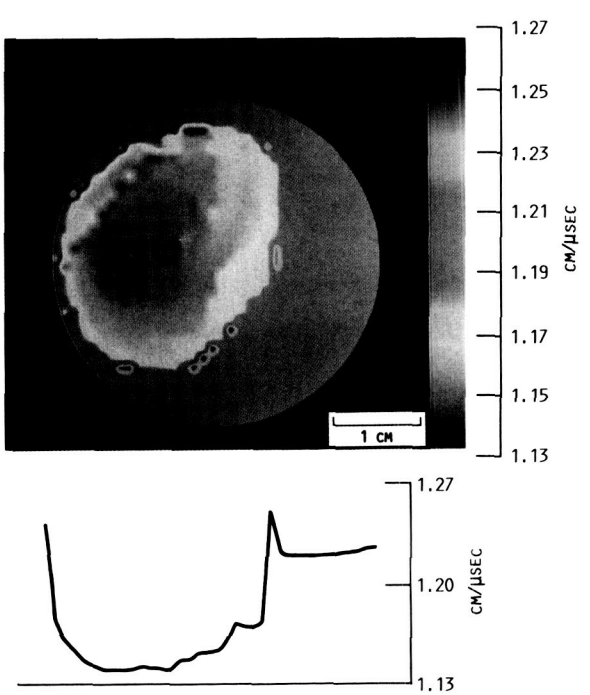

Figure 12.—Cross correlation velocity map of SiC disk sintered at 2190 °C. (CD-87-26961)

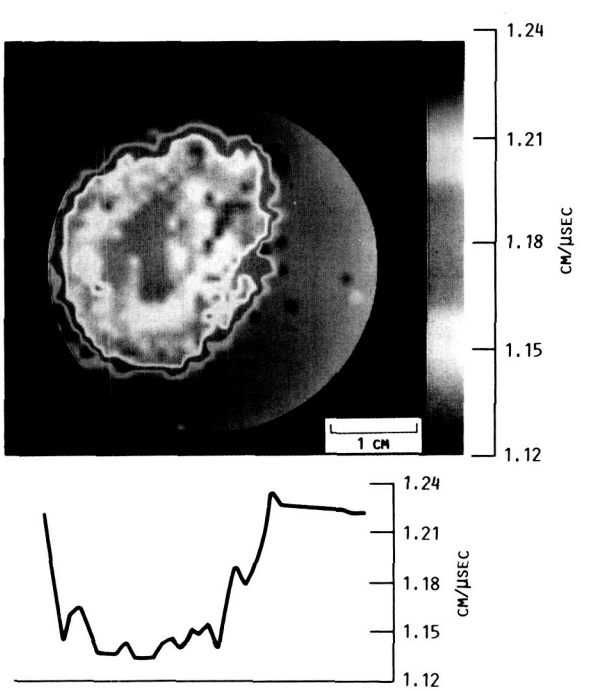

Figure 13.—Phase velocity map of SiC disk sintered at 2190 °C. (CD-87-26962)

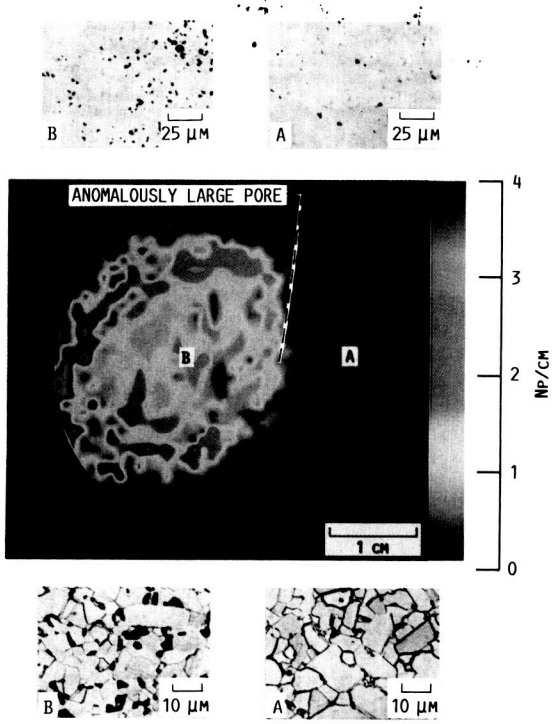

Figure 14.—Attenuation map at 100 MHz and microstructure for SiC disk sintered at 2190 °C. (CD-87-26963)

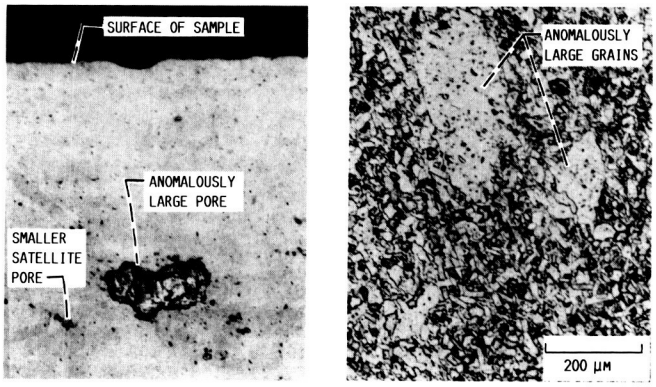

Figure 15.—Anomalously large pore and grains observed in the SiC disk sintered at 2190 °C. (CD-87-26974)

the line passing through points A and B. In this same path, an anomalously large pore surrounded by smaller satellite pores, was found (fig. 15) at the right hand edge of the high attenuation region.

The sample generally reveals a reflection coefficient (fig. 16) in the range 0.3 to 0.55. The two large horizontal bands near the center correspond to reflection coefficients in the range 0.7 to 0.85. They are, for the most part, within range to yield accurate results. There are also, dilute, isolated regions, positioned at the outer edge of the high attenuating region, exhibiting a low reflection coefficient. These areas will yield attenuation results that are of questionable validity.

ORIGINAL PAGE
COLOR PHOTOGRAPH

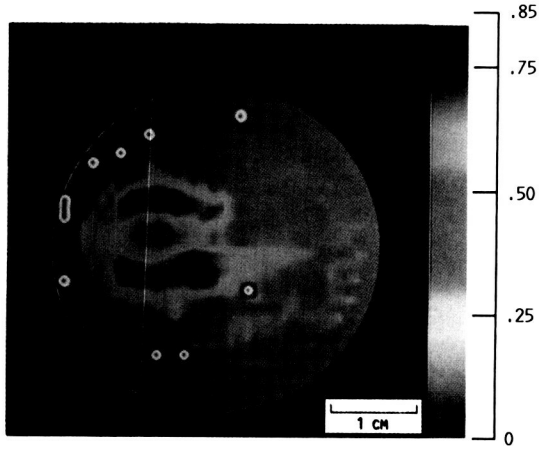

Figure 16.—Reflection coefficient map at 100 MHz for SiC disk sintered at 2190 °C. (CD-87-26965)

Discussion

The velocity and attenuation maps clearly indicate higher sensitivity to microstructural variations than the radiographic results. This is quite dramatic, particularly for the sample sintered at the lower temperature. The phase velocity maps revealed a more detailed image than the cross-correlation maps. This is a result of the averaging or smoothing effect implicit in the cross-correlation calculation where all frequency components of the waveforms are used to determine a single group-like velocity.

In the attenuation map (fig. 14) we have observed extremely low attenuation (at 100 MHz) at point A (most dense region) where there exist large grains. Therefore, grain boundary scattering can be ruled out as a dominant attenuation mechanism for frequencies up to 100 MHz for SiC containing grain sizes ranging from 5 to 15 μm. This implies that each of the attenuation maps shown in this work is a map of attenuation due to scattering at the pore sites. Also at point A we have the highest velocity, therefore, increases in velocity correspond to higher densities.

Consider figures 5, 6, and 8, at point A (with high velocity and high attenuation) we have a dense region with large pores, while at point B (with low velocity and low attenuation) we have a less dense region with smaller pores. The difference in porosity fraction between points A and B is 5 percent. The difference in the maximum pore size (excluding anomalously large pores) between points A and B is 500 percent. When comparing this to the variation in phase velocity of 4.5 percent and attenuation of 100 percent, between the two points, a general correlation is observed. The velocity is sensitive to the local porosity fraction and the attenuation is sensitive to the local pore size. That is, higher velocities correspond to denser regions and higher attenuation corresponds to regions with larger pores. So that for a "clean" ceramic having a very

high density and small pore size we would expect to find very high velocity and low attenuation values. This is observed in the higher density sample at point A in figures 12 to 14. (It should be pointed out this is only a generalization and that pore clustering, pore size distribution, numerical number of pores, etc. may have to be considered.) These results are consistent with previous work (ref. 10). The actual correlation function is not known but may be obtained by determining the quantitative porosity size distribution function everywhere throughout the bulk of the sample. This is a formidable task requiring computer controlled, precision measurements of pore size.

Conclusion

Acoustic images of silicon carbide ceramic disk were obtained using a precision scanning contact pulse echo technique. Phase and cross-correlation velocity, and attenuation maps were used to form color images of microstructural variations. These acoustic images revealed microstructural variations not observable with x-ray radiography.

References

1. D.W. Richardson, Modern Ceramic Engineering: Properties, Processing and Use in Design, (Marcel Dekker, New York, 1982) Ch. 3.
2. S. Dutta, "Sinterability, Strength and Oxidation of Alpha Silicon Carbide Powders," J. Mater. Sci., 19, 1307 (1984).
3. S. Dutta, "Strength Optimization of a-SiC By Improved Processing," Structural Ceramics, NASA CP-2427, (NASA, Washington, D.C., 1986) pp. 89-98.
4. W.A. Sanders, and G.Y. Baaklini, "Correlation of Processing and Sintering Variables with the Strength and Radiography of Silicon Nitride," Ceram. Eng. Sci. Proc., 7, 839 (1986).
5. S.J. Klima, and G.Y. Baaklini, "Ultrasonic Characterization of Structural Ceramics," Analytical Ultrasonics in Materials Research and Testing, NASA CP-2383, (NASA, Washington, D.C., 1986) pp. 117-126.
6. G.Y. Baaklini, E.R. Generazio, and J.D. Kiser, "High Frequency Ultrasonic Characterization of Sintered SiC," presented at the 11th Annual Conference on Composition and Advanced Ceramic Materials, Jan. 18-23, 1987, Cocoa Beach, FL.
7. E.R. Generazio, "The Role of the Reflection Coefficient in Precision Measurement of Ultrasonic Attenuation," Mater. Eval. 43, 995 (1985).
8. D.R. Hull, H.E. Kautz, and A. Vary, "Measurement of Ultrasonic Velocity Using Phase-Slop and Cross-Correlation Methods," Mater. Eval., 43, 1455 (1985).
9. W. Sachse, and Y.H. Pao, "On the Determination of Phase and Group Velocities of Dispersive Waves in Solids," J. Appl. Phys., 39, 4320 (1978).
10. A.G. Evans, B.R. Tittman, L. Ahlberg, B.J. Khuri-Yakub, and G.S. King, "Ultrasonic Attenuation in Ceramics," J. Appl. Phys. 49, 2669 (1978).

NASA
National Aeronautics and Space Administration

Report Documentation Page

1. Report No. NASA TM-100129	2. Government Accession No.	3. Recipient's Catalog No.
4. Title and Subtitle Imaging Subtle Microstructural Variations in Ceramics With Precision Ultrasonic Velocity and Attenuation Measurements		5. Report Date November 1987 6. Performing Organization Code 506-43-11
7. Author(s) Edward R. Generazio, Don J. Roth, and George Y. Baaklini		8. Performing Organization Report No. E-3710 10. Work Unit No.
9. Performing Organization Name and Address National Aeronautics and Space Administration Lewis Research Center Cleveland, Ohio 44135-3191		11. Contract or Grant No. 13. Type of Report and Period Covered Technical Memorandum
12. Sponsoring Agency Name and Address National Aeronautics and Space Administration Washington, D.C. 20546-0001		14. Sponsoring Agency Code

15. Supplementary Notes

Material previously presented at the Review of Progress in Quantitative NDE, sponsored by Iowa State University, Williamsburg, Virginia, June 21-26, 1987.

16. Abstract

Acoustic images of silicon carbide ceramic disk were obtained using a precision scanning contact pulse echo technique. Phase and cross-correlation velocity, and attenuation maps were used to form color images of microstructural variations. These acoustic images reveal microstructural variations not observable with x-ray radiography.

17. Key Words (Suggested by Author(s)) Ultrasonic; Imaging; Silicon carbide; Silicon nitride; Ultrasonic velocity; Ultrasonic attenuation; Acoustic microscopy	18. Distribution Statement Unclassified–Unlimited Subject Category 38

19. Security Classif. (of this report)	20. Security Classif. (of this page)	21. No of pages	22. Price*
Unclassified	Unclassified	10	A02

NASA FORM 1626 OCT 86

*For sale by the National Technical Information Service, Springfield, Virginia 22161